Diffusion of nanosized sodium inclusions in platinum

1994 J. Phys.: Condens. Matter 6 5397

(http://iopscience.iop.org/0953-8984/6/28/014)

J. Phys.: Condens. Matter 6 (1994) 5397–5408. Printed in the UK

Diffusion of nanosized sodium inclusions in platinum

J R Poulsen†, A Horsewell†, M Eldrup†, E Johnson‡ and A Johansen‡

† Materials Department, Risø National Laboratory, DK-4000 Roskilde, Denmark

‡ The Niels Bohr Institute for Astronomy, Physics and Geophysics, Ørsted Laboratory, Universitetsparken 5, DK-2100 Copenhagen Ø, Denmark

Received 10 February 1994

Abstract. Na inclusions with diameters in the range from 2 nm to 15 nm have been made by ion implantation of Na into 70 nm thick single-crystalline Pt foils followed by annealing. The structure of solid inclusions and the diffusion of molten inclusions have been studied by transmission electron microscopy. At room temperature the inclusions are faceted and crystalline with a BCC structure and they are aligned topotactically with the Pt (FCC) matrix. The diffusion of inclusions in the liquid state was investigated by annealing at temperatures of 1227 K, 1432 K and 1534 K. The diffusion coefficient was found to have a dependence on the inclusion radius and an activation energy of 2.8 ± 0.2 eV, this being consistent with a mechanism by which volume self-diffusion of Pt controls the diffusion rate of the inclusions. Diffusion of Pt at the interfaces between the Pt matrix and the liquid Na inclusions was found to be strongly inhibited compared with the free surface self-diffusion of Pt. The results are used to propose a method to produce sources for positron annihilation spectroscopy at high temperatures.

1. Introduction

Interest in nanosized metal inclusions has focused mainly on their structure and on the melting and solidification processes. When the inclusions are crystalline and embedded in a crystalline matrix, a strong influence of the surrounding matrix on the inclusions often results in a topotactical alignment of the inclusions with the matrix. Some examples with a cube/cube alignment are Pb inclusions in Al (Gråbaek *et al* 1989), Na inclusions in Al (Horsewell 1990) and K inclusions in W (Kim and Welsch 1990). Topotactical alignment may occur even though the misfit across the inclusion–matrix interface is large and the interface is incoherent (Horsewell *et al* 1993). In addition to being topotactically aligned, small inclusions may also adopt the same crystal structure as the matrix as seen for example in the immiscible systems Al–In (Silcock 1955/56), Cu–K, Mo–Kr (Templier 1991) and Al–Tl (Johnson *et al* 1993). The embedded inclusions are generally pressurized and there is often a strong influence on melting and solidification temperatures (Gråbaek *et al* 1990, Zhang and Cantor 1990).

Although it may be of great relevance for the study of the inclusion–matrix interfaces and the thermal properties of inclusions, no quantitative investigation of the diffusion of immiscible metal inclusions has to our knowledge been reported. In contrast, diffusion of noble gas bubbles (i.e. inclusions with noble gas in the solid, liquid or gaseous state) in metals is a well studied problem and it is known that bubble diffusion may be controlled by one or a combination of different mechanisms for atomic diffusion (Nichols 1969, Goodhew and Tyler 1981). For example, Yamaguchi *et al* (1989) have observed diffusion of solid and liquid Kr bubbles in Al and interpreted the diffusion rate as being controlled by volume diffusion, i.e. the rate controlling mechanism was volume self-diffusion of matrix atoms via

0953-8984/94/285397+12$19.50

thermal vacancy migration around the bubbles. Evans and van Veen (1989) on the other hand, found that diffusion of He bubbles in Au was surface diffusion controlled, i.e. the rate controlling mechanism was self-diffusion of matrix atoms on the interior bubble surfaces.

In the present work we have used to a novel method based on ion implantation of very thin foils to study the thermal diffusion of inclusions in a matrix. The method gives information on both the inclusion size and the temperature dependence of the diffusion rate. Thin Pt foils, ion implanted with Na, were annealed and then observed in a transmission electron microscope (TEM). The observations show the changes in the size distribution of the Na inclusions due to the diffusion of the inclusions to the foil surfaces. Comparison of the present data with models previously used to describe gas bubble diffusion strongly suggests that the diffusion of the inclusions is controlled by volume self-diffusion of Pt.

An additional motivation for carrying out the present investigations is our ambition to produce sources for positron annihilation spectroscopy that can be used at high temperatures. A suitable source may be produced by ion implantation of the positron emitter ^{22}Na into Pt, which has a high melting point and is oxidation resistant (Ravn *et al* 1991).

2. Experimental procedures

Pt (100) single-crystal foils were prepared (by J Chevallier, Aarhus University) with a thickness of 70 nm from 99.99% pure Pt by electron gun evaporation onto NaCl (100) air cleaved surfaces, maintained at a temperature of 360 °C. The pressure during evaporation was about 5×10^{-7} Torr. The thickness of the foils and the rate of evaporation, adjusted to 1 nm s^{-1}, were controlled within ±10% by an oscillating quartz film thickness monitor. After the NaCl backings were dissolved, the foils were cleaned with double-distilled Millipore water and mounted between double Pt TEM grids for the remaining experimental procedures. The foils were implanted at room temperature with 60 keV Na^+ ions to a fluence of 1×10^{16} cm^{-2} using a low beam current of 0.3 μA cm^{-2} in order to minimize beam heating of the foils. The depth profile of the concentration of implanted Na as determined by a Monte Carlo simulation using TRIM version 90 (Ziegler *et al* 1985) is shown in figure 1. A fraction of 22% of the ions were back scattered and a fraction of 8% of the ions were transmitted in the simulation. After implantation, the foils were annealed in a vacuum of about 5×10^{-7} Torr at 1227 K, 1432 K and 1534 K (0.6, 0.7 and 0.75 times the melting temperature, T_M, for Pt) for 1 h at each temperature. The temperatures were controlled within ±5 K and heating and cooling rates of 20 K min^{-1} were used. The annealing temperatures are so much higher than the bulk melting point of Na, 390 K, that all the inclusions must have been melted during the full annealing periods. After each anneal, the foils were studied at room temperature without any further preparation in a JEOL 2000FX TEM operated at 200 kV.

3. Results

The as implanted Pt foils had a high density of radiation damage which made it impossible to observe any Na inclusions in the TEM. Figure 2(*a*) shows a TEM micrograph of a Pt foil after annealing at 1227 K. Only very few dislocations but a high density of Na inclusions with diameters in the range from 2 nm to 15 nm are now visible. The inclusions are faceted with polyhedral regular shapes, all having the same orientation in the matrix. Figure 2(*b*) and (*c*) shows TEM micrographs of the Pt foil after annealing at 1432 K and 1534 K,

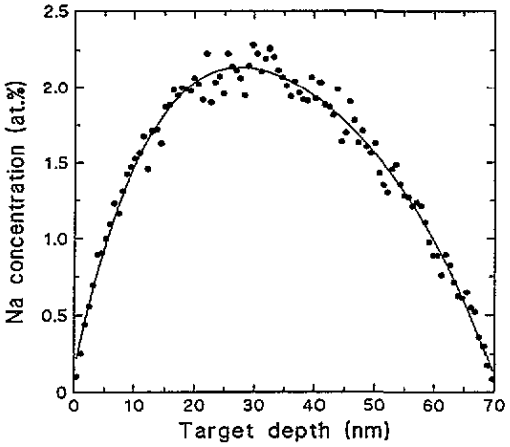

Figure 1. The depth profile of Na in a 70 nm thick Pt foil implanted with 60 keV Na^+ ions to a fluence of 1×10^{16} cm^{-2}. The line is a guide for the eye. The profile was simulated by use of the TRIM-90 program.

respectively. The only visible change from the annealing at 1227 K is a reduction in number of the smallest Na inclusions. The concentration of Na was too low and the ratio between the electron densities in Na and Pt too small to give visible selected area diffraction spots from the inclusions. It was therefore not possible to determine the crystal structure of the inclusions and their alignment relation with the Pt (FCC) matrix from the diffraction patterns. Nevertheless, strong two-beam bright-field micrographs showed moiré fringes on Na inclusions. These fringes were along Pt ⟨001⟩ directions, with spacings of ~ 1.15 nm. This is consistent with Pt {022} producing parallel moiré interference fringes with Na {222}. The fringe spacing shows undistorted, non-pressurized BCC Na inclusions aligned topotactically with the Pt matrix. Further analysis of Na inclusion orientation is currently in progress. Some indication of the existence of a Pt_2Na cubic Laves phase with a lattice parameter of ~ 0.75 nm has been reported (Nash *et al* 1960). However, that the inclusions could be a Pt_2Na phase is inconsistent with both the moiré fringe spacing and the mass–thickness contrast observed (figure 2(*c*)).

Figure 3 shows the size distributions of Na inclusions in the Pt foils after annealing at 1227 K, 1432 K and 1534 K, as determined by direct measurements on prints of the TEM micrographs enlarged to a magnification of 3×10^5. The radii used in the figure and in the following discussion are determined as half the projected dimension in the Pt ⟨001⟩ directions. The most distinct feature of the distributions is the progressive disappearance of the smaller inclusions by annealing at the higher temperatures.

Using the measured diameters to calculate the volumes of the inclusions in a spherical approximation, the inclusions were estimated to contain total amounts of Na equal to retained fractions of about 5%, 4% and 3% of the implanted Na after annealing at 1227 K, 1432 K and 1534 K, respectively. The main part of the implanted Na had probably diffused to the foil surfaces in the early annealing stages, as will be discussed later.

4. Discussion

The straightforward explanation of the disappearance of the smaller inclusions (figure 3) is that they had migrated to the foil surfaces where the Na evaporated. Coalescence of the

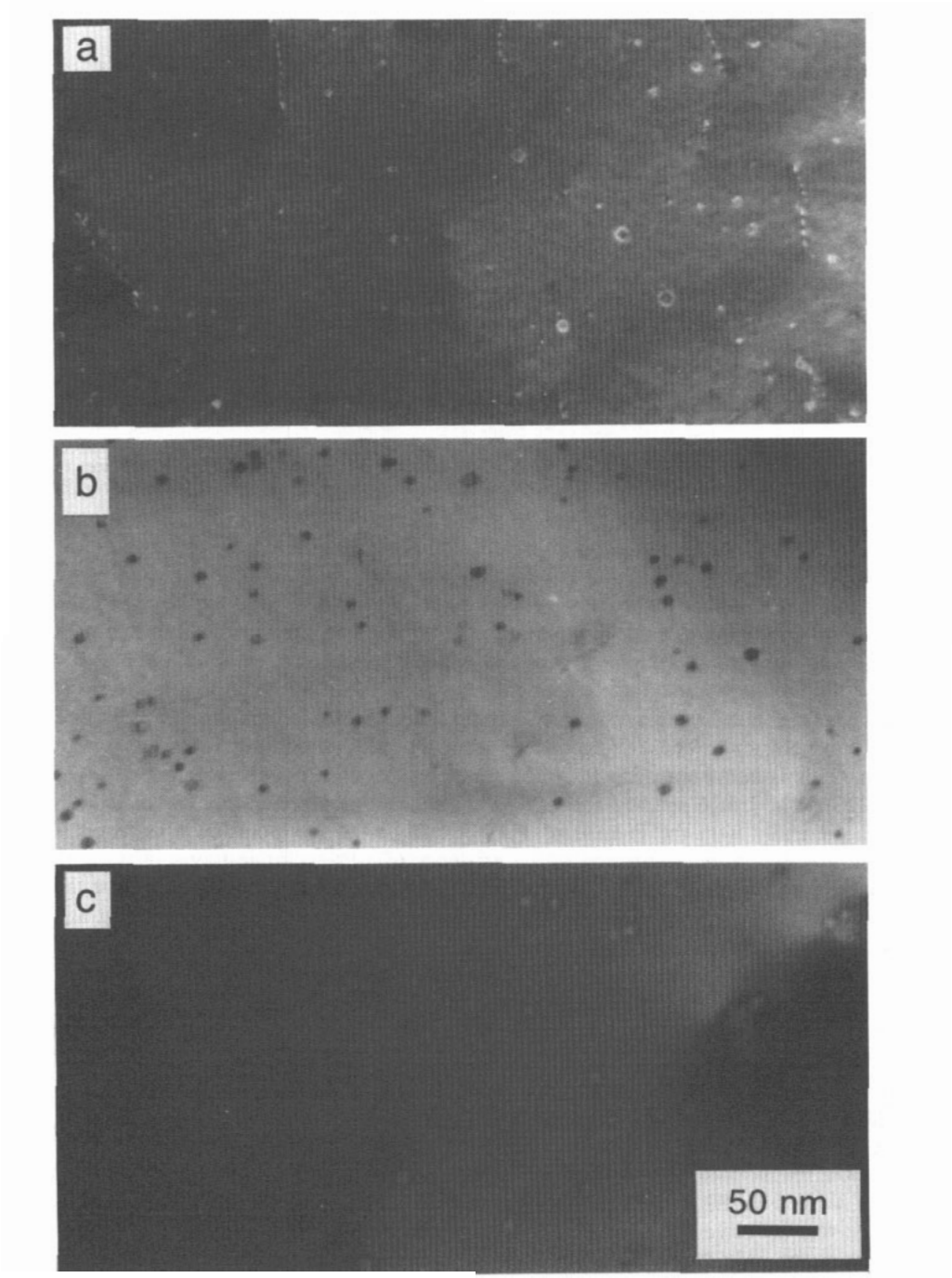

Figure 2. TEM micrographs of an ion implanted foil: (*a*) annealed at 1227 K ($0.6T_m$) for 1 h; (*b*) further annealed at 1432 K ($0.7T_m$) for 1 h; (*c*) finally annealed at 1534 K ($0.75T_m$) for 1 h. The micrographs illustrate typical contrasts for the various imaging conditions used: (*a*) weak-beam dark field; (*b*) bright field, Na particles strongly diffracting; (*c*) kinematical image (many beam), mass–thickness contrast.

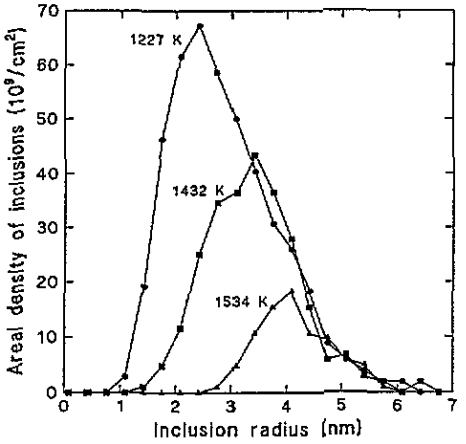

Figure 3. The size distributions of Na inclusions in an ion implanted foil annealed at 1227 K for 1 h (circles), further annealed at 1432 K for 1 h (squares) and finally annealed at 1534 K for 1 h (triangles). The inclusion radii are sorted into classes with a width of $\frac{1}{3}$ nm. A total of 300–500 inclusions were measured for each temperature. The data for inclusions with a radius below about 1.5 nm may be erroneous due to their poor visibility in the TEM micrographs.

inclusions is negligible for annealing above 1227 K because the mean distance between the inclusions (about 43 nm after annealing at 1227 K) is of the same magnitude as the foil thickness. This is similar to the observations of Evans and van Veen (1989), who observed no bubble coalescence but only bubble diffusion to the surface of an Au specimen with a mean density of about 2×10^{18} bubbles cm^{-3} in a 6 nm ion implanted layer. The present conditions with a mean density of about 1.3×10^{16} inclusions cm^{-3} after the 1227 K anneal are more favourable for non-coalescence. Accepting that the changes in the observed size distributions of the Na inclusions are due to diffusion of the inclusions to the foil surfaces, the size distributions can be analysed in a simple one-dimensional diffusion model from which the diffusion coefficient for the Na inclusions can be obtained.

4.1. One-dimensional diffusion

It is assumed that the number density of inclusions of each radius is distributed through the Pt foil with a sinusoidal density profile. This assumption is made because the concentration profile of Na in the as implanted foil is seen to be close to sinusoidal (figure 1) (the Gaussian profile often observed for deep implantations is very distorted by the presence of the surfaces) and upon annealing it rapidly approaches this shape (Schmalzried 1974). Solving the diffusion equation on this assumption results in a sinusoidal density profile with exponential time decay for inclusions with a given radius r (Schmalzried 1974):

$$C_r(x,t) = (\pi/2)c_r^0 \sin((x/L)\pi)\exp(-(\pi^2/L^2)D_i(r)t) \qquad 0 \leqslant x \leqslant L \quad (1)$$

where x is the depth from one of the surfaces, t is the annealing time, c_r^0 is the mean density of inclusions with radius r at time $t = 0$, L is the foil thickness and $D_i(r)$ is the diffusion coefficient of the inclusions with radius r. Integration over x gives the areal density of inclusions with radius r:

$$C_r(t) = c_r^0 L \exp(-(\pi^2/L^2)D_i(r)t). \quad (2)$$

Using the initial areal density, $C_r(0) = c_r^0 L$, substituting L by $L - 2r$, the effective foil thickness (since the inclusions evaporate as soon as they touch the foil surfaces), and solving for $D_i(r)$, results in the equation

$$D_i(r) = -[(L - 2r)^2/\pi^2 t] \ln[C_r(t)/C_r(0)] \tag{3}$$

from which the diffusion coefficient can be calculated using the data shown in figure 3. Take, for example, inclusions with radius 1.75 nm. The areal density of these inclusions after the 1432 K anneal is $C_{1.75}(3600\ \text{s}) = 4.9 \times 10^9\ \text{cm}^{-2}$ and before the 1432 K anneal (i.e. after the 1227 K anneal) $C_{1.75}(0) = 46 \times 10^9\ \text{cm}^{-2}$ (figure 3). From (3) we obtain $D_i(1.75\ \text{nm}) = 28 \times 10^{-16}\ \text{cm}^2\ \text{s}^{-1}$. Figure 4 shows the diffusion coefficients for various sizes determined in this way using (3) and the data shown in figure 3.

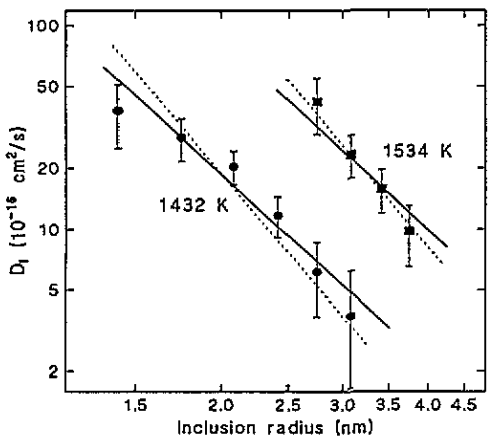

Figure 4. The size dependence of the diffusion coefficient for Na inclusions in Pt. The circles and the squares are experimental values for temperatures of 1432 K and 1534 K, respectively. The full lines represent a least-squares fit of the volume diffusion model (4) and the dotted lines a least-squares fit of the surface diffusion model (5) to the data.

4.2. Volume and surface diffusion

Several different diffusion mechanisms have been considered in earlier discussions of rare gas bubble diffusion in metals (see Goodhew and Tyler 1981). In most cases, either volume diffusion or surface diffusion of matrix atoms has been found to control the bubble diffusion rate. In the following we shall discuss these mechanisms in relation to the present results. The bubble diffusion coefficient $D_i(r)$ is expressed by the following equations (Nichols 1969):

$$D_i(r) = (3\Omega/4\pi r^3) D_v \tag{4}$$

for volume diffusion control, and

$$D_i(r) = (3\Omega^{4/3}/2\pi r^4) D_s \tag{5}$$

for surface diffusion control. Here, r is the bubble radius, Ω is the atomic volume of the matrix ($1.51 \times 10^{-23}\ \text{cm}^3$ for Pt), D_v is the volume self-diffusion coefficient and D_s is the

surface self-diffusion coefficient of the matrix atoms, both assumed to be simple activated diffusion processes of the form $D = D_0 \exp(-E/kT)$. Apart from a probably moderate difference in the rate of exchange of Pt vacancies with a free surface compared to that of an interface with liquid Na, there are no premises that limit the use of (4) for liquid Na inclusions. Equation (4) has therefore been fitted to the experimental diffusion coefficients using a weighted least-squares method with D_0 and E as fitting parameters. An activation energy of $E = 2.8 \pm 0.2$ eV is found from the fit, and the best fit, represented with full lines in figure 4, is given by

$$D_i(r) = 7.2 \times 10^{-3}(\Omega/r^3)\exp(-2.8 \text{ eV}/kT) \text{ cm}^2 \text{ s}^{-1}.$$

By using the Pt volume self-diffusion coefficient of Rein *et al* (1978),

$$D_v = (5 \pm 2) \times 10^{-2} \exp((-2.67 \pm 0.05) \text{ eV}/kT) \text{ cm}^2 \text{ s}^{-1}$$

the diffusion coefficient of the Na inclusions, as theoretically determined by (4), is

$$D_i(r) = (1.2 \pm 0.5) \times 10^{-2}(\Omega/r^3)\exp(-(2.67 \pm 0.05) \text{ eV}/kT) \text{ cm}^2 \text{ s}^{-1}.$$

The activation energy of 2.67 ± 0.05 eV is in good agreement with the value of 2.8 ± 0.2 eV of the present study. However, the calculated value of D_i is higher than the present experimental values (figure 4) by a factor of three to six. This deviation is probably too high to be explained by experimental inaccuracies but, as mentioned, the exchange rate of Pt vacancies with the Pt–Na interface could well be somewhat lower than the exchange rate with a free surface.

Even though the diffusion of the Na inclusions is well explained by Pt volume self-diffusion as expressed in (4), it is interesting to examine the possible role of Pt diffusion at the Pt–Na interfaces for the diffusion of the Na inclusions. For this, a weighted least-squares fit has also been made of (5) to the experimental diffusion coefficients (figure 4). The best fit is shown as dotted lines in figure 4. The activation energy estimated by the fit, $E = 3.6 \pm 0.3$ eV, is clearly too high for diffusion of Pt at the Pt–Na interfaces; it should not be higher but probably lower than the activation energy for Pt volume self-diffusion. The failure of the fit to give a realistic value of the activation energy shows that diffusion of Pt at the Pt–Na interfaces is of no importance in controlling the diffusion of the Na inclusions. Taking the Pt (100) free surface self-diffusion coefficient from Kellog (1991)

$$D_s = 1.3 \times 10^{-3} \exp(-0.47 \text{ eV}/kT) \text{ cm}^2 \text{ s}^{-1}$$

equation (5) gives a value of D_i about six orders of magnitude higher than the experimental values determined by the present study. In fact, all the inclusions would have diffused to the surfaces and evaporated during the annealing at 1227 K if D_i had such a high value. The deviation is similarly high when Pt self-diffusion coefficients for other surface planes (Liu *et al* 1991) are used in (5). A reasonable explanation for this enormous overestimate of D_i is that Pt diffuses much more slowly at the Pt–Na interfaces than on free Pt surfaces. Mikhlin (1979) has proposed that He bubbles under high pressure (and thereby with a high He density) will in some cases have a diffusion coefficient several orders of magnitude below the value determined by (5) because the high density of He in the bubbles can lead to a strong blocking of the jumps of matrix atoms on the bubble surfaces. Along the same lines, the absence of Pt surface self-diffusion as a rate controlling mechanism may be explained

by the relatively high density of Na in the liquid inclusions leading to an effective blocking of Pt diffusion at the Pt–Na interfaces.

Another mechanism, which in some cases is known to limit the diffusion rate of faceted rare gas bubbles, is the ledge nucleation limited bubble diffusion given by (Goodhew and Tyler 1981)

$$D_i(r) = (D_s r/\alpha)\exp(-\pi r\epsilon/kT) \tag{6}$$

where D_s is the surface self-diffusion coefficient as in (5), α is the atom jump distance ($\sim$ 0.28 nm for Pt), and ϵ is the energy per unit length of a monoatomic ledge on the bubble facets. (6) has been fitted to the experimental results shown in figure 4 with the results $D_s = 3 \times 10^{-5}\exp(-2.7\ \text{eV}/kT)\ \text{cm}^2\ \text{s}^{-1}$ and $\epsilon = 0.078\ \text{eV nm}^{-1}$. Using this value of D_s in (5), results in calculated values of D_i three to four orders of magnitude lower than the corresponding values of D_i calculated from (6). This means that nucleation of ledges does not, in the present case, reduce the diffusion rate of the Na inclusions by limiting their surface diffusion. It should also be noted that even though the inclusions were faceted at room temperature they could well have been rounded at the temperatures used for the anneals.

Diffusion of inclusions by the above mechanisms (4)–(6) presupposes the inclusions not to be solid so that they can easily assume the shape of the surrounding matrix on an atomic scale (Nichols 1969, Goodhew and Tyler 1981), whereas solid inclusions will hardly move when a few matrix atoms and vacancies rearrange at the matrix–inclusion interfaces. Similarly, Jensen *et al* (1988) proposed that Kr bubbles in Cu and Ni could not diffuse at low temperatures because the presence of solid Kr prevented normal bubble migration mechanisms. Furthermore, Schmidt (1992) has observed by *in situ* heating in TEM that the mobility of Pb inclusions in Al increase considerably upon melting of the Pb inclusions at a fixed temperature. This suggests that the diffusion of the Na inclusions would cease when the inclusions become solid. However, the bulk melting point of Na (390 K) is much lower than that of Pt, and the solidification of Na will therefore only influence the diffusion at temperatures much lower than those used in the present study.

Recently, Van Siclen and Wright (1993) have proposed that the diffusion of He bubbles in Al may be enhanced if the interior surfaces of the bubbles are coated with a layer of liquid Pb or In. It is conjectured that the enhancement is caused by a rapid diffusion of matrix atoms through the liquid metal coatings. The analogous process in the present case will be diffusion of Pt atoms through the liquid Na inclusions. If the diffusion of the Na inclusions is controlled by this mechanism, the diffusion coefficient of the inclusions is given by (Van Siclen and Wright 1993)

$$D_i(r) = (3\Omega^2/8\pi r^3)c_{\text{Pt,Na}}D_{\text{Pt,Na}} \tag{7}$$

where $c_{\text{Pt,Na}}$ is the equilibrium concentration of Pt in Na and $D_{\text{Pt,Na}}$ is the diffusion coefficient for Pt in Na. The values of both $c_{\text{Pt,Na}}$ and $D_{\text{Pt,Na}}$ are unknown, so it is impossible to estimate D_i from (7), but, as mentioned, the experimental results are well explained by the volume diffusion mechanism (4). It seems, therefore, that diffusion of Pt through the Na inclusions only contributes negligibly to D_i. This makes it possible, by equating (7) to about one fifth of the experimental values, to estimate upper limits of the product of the concentration of Pt in liquid Na and the diffusion coefficient for Pt through liquid Na: $c_{\text{Pt,Na}}D_{\text{Pt,Na}} \leqslant 1 \times 10^{11}\ \text{cm}^{-1}\ \text{s}^{-1} \simeq 1 \times 10^{-12}$ at.% $\text{cm}^2\ \text{s}^{-1}$ at 1432 K and $c_{\text{Pt,Na}}D_{\text{Pt,Na}} \leqslant 1 \times 10^{12}\ \text{cm}^{-1}\ \text{s}^{-1} \simeq 1 \times 10^{-11}$ at.% $\text{cm}^2\ \text{s}^{-1}$ at 1534 K.

4.3. Ostwald ripening

A quite different mechanism that can lead to a coarsening of bubbles and other precipitates in bulk metals without direction migration is the so called Ostwald ripening mechanism. The basic process for this mechanism is an exchange of precipitate atoms between the matrix and the precipitates. The dissociation rate is faster than the association rate for the smaller precipitates, which will shrink, and vice versa for the larger precipitates, which will grow (Markworth 1973). In discussing Ostwald ripening in relation to the Na inclusions in the Pt foils, the role of the foil surfaces must be considered. Because the mean distance between the inclusions is comparable with the foil thickness, Na atoms dissociated from the inclusions will have a high probability of reaching the foil surfaces and thus evaporate before they become associated to another inclusion. This means that all the inclusions as well as their mean size will shrink if migration of the inclusions can be neglected. The actual growth of the mean size of the inclusions observed in the present study (figure 3) therefore strongly suggests that dissociation of Na from the inclusions is of minor or no importance for the observed changes in the distributions of the inclusion sizes (figure 3). This leaves the volume diffusion as the dominating mechanism controlling the diffusion of Na inclusions in Pt.

4.4. Stability of Na inclusions

As mentioned in section 3, only a small fraction, above 5% of the implanted Na, was retained in the inclusions after annealing at 1227 K whereas the major part, about 95% of the implanted Na, had diffused out of the foil or was dissolved in the Pt matrix. In order to study this in more detail, one of the ion implanted foils was annealed at 1023 K ($0.5T_m$) for 1 h. Figure 5 shows a TEM micrograph of this foil. It has a high density of Na inclusions, many with very irregular shapes and only partially faceted surfaces. The dislocations produced by the ion implantation were only partly annealed out of the foil (the density is about 1×10^{10} dislocations cm^{-2}) and many of the inclusions are seen to be attached to dislocations. Some of the inclusions are very large, with diameters up to about 25 nm. A fraction of about 40% of the implanted Na is estimated to be retained in the inclusions. After a further annealing at 1227 K for 1 h, the foil contained only Na inclusions with regular well faceted shapes and the size distribution of the inclusions was similar to that shown for the same temperature in figure 3. This indicates that with the implantation conditions used, a minimum temperature of about 1100–1200 K is necessary to produce well faceted Na inclusions with regular shapes in a well annealed Pt matrix. The high density of radiation damage (vacancies, dislocations etc) in the Pt foils produced during ion implantation is expected to increase Pt self-diffusion, therefore increasing the mobility of Na, and may further promote dissociation of loosely bound Na from the irregular inclusions. Both these mechanisms may contribute to the considerable loss of Na observed at about 1100–1200 K.

Such a behaviour is in qualitative agreement with recent experiments of Uhrmacher and Lieb (1992). They used the $^{23}Na(p, \gamma)^{24}Mg$ resonant nuclear reaction to make annealing studies of the depth profiles of implanted Na in a variety of metals. Their method could not distinguish between Na atoms dissolved in the matrix and Na precipitated into inclusions, but its advantage is its ability to measure the depth profile of all the Na present in the samples. They found that the retained fraction of implanted Na was close to 100% after annealing for 30 min at all temperatures below a 'critical temperature', T_c. Upon annealing at temperatures in a narrow interval around T_c, the retained fraction of implanted Na changed rapidly with temperature to a value of about 5–10%. T_c was found to be about $0.5T_m$ for the

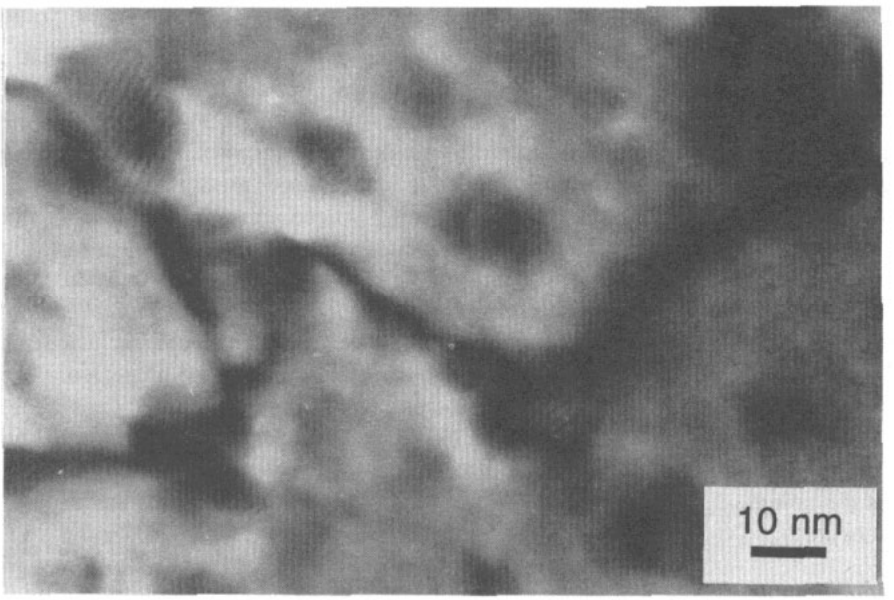

Figure 5. A TEM micrograph of an ion implanted foil annealed at 1023 K ($0.5T_m$) for 1 h. The Na inclusions have mainly {001} facets and show parallel moiré fringes along {011} directions. The moiré fringe spacing is ~ 1.15 nm, this being consistent with Pt {022}‖Na{222}.

BCC metals Fe, Cr and Mo and about $0.7T_m$ for the FCC metals Ni and Al. It is interesting to note that, although the same qualitative behaviour is observed in the present work, the T_c for FCC Pt is only $0.5–0.6T_m$. This shows that there are no simple relationships between T_c and the lattice structure. Although not discussed by the authors, the retained fraction of about 5–10% of the implanted Na remained in the samples even after annealing at the highest temperatures, as can be seen from figure 6 of Uhrmacher and Lieb (1992).

Thus it seems that at sufficiently high temperatures about 5–10% of the implanted Na forms inclusions that are stable with regular shapes, which then only diffuse slowly at high temperatures in a well annealed matrix. This condition is reached after 90–95% of the implanted Na has diffused out of the matrix.

Finally, the present investigation shows that stable ^{22}Na positron sources for use at much higher temperatures than the ~ 900 K limit for standard ^{22}NaCl sources (MacKenzie 1983) may be made by ion implantation of ^{22}Na into Pt foil followed by an annealing at about 1500 K to release the smaller inclusions. The loss of ^{22}Na by diffusion will then be very slow if the source is used at temperatures below 1300 K, and the Pt foil ensures that the source is resistant to oxidation. We are planning to make positron sources using this approach.

5. Summary and conclusions

The use of TEM transparent Pt foils for Na ion implantation and subsequent annealing treatments has made it possible to study the formation of Na inclusions in Pt by TEM and analyse in detail the diffusion of the inclusions in a simple one-dimensional model.

A few per cent of the implanted Na forms well faceted unpressurized inclusions with a BCC structure topotactically aligned with the Pt (FCC) matrix after annealing at temperatures

above 1227 K. The main part of the implanted Na diffuses out of the foils during an earlier annealing stage. The liquid Na inclusions diffuse with a rate that is well described by a Pt volume diffusion controlled mechanism (4) when the exchange rate of Pt vacancies with the Pt–Na interfaces is supposed to be about one quarter of the exchange rate with a free Pt surface. Diffusion of Pt at the Pt–Na interfaces is strongly suppressed compared with the expected diffusion on a free Pt surface because of the presence of Na at the interfaces. This results in only a negligible contribution from Pt interface diffusion to the total diffusion rate of the Na inclusions. The other mechanisms studied, ledge nucleation limited diffusion and Ostwald ripening, are also found to be negligible processes compared with the volume diffusion controlled mechanism.

Equation (4) may be used to estimate the diffusion coefficient of liquid inclusions in other metallic inclusion–matrix systems above the melting temperature of the inclusions, when diffusion of matrix atoms at the interfaces can be neglected because of the high density of inclusion atoms at the interfaces.

Finally, the present results have been used to propose a method for producing positron sources for use at high temperatures.

Acknowledgments

We would like to thank J Chevallier, Institute of Physics and Astronomy, Aarhus University, for the production of the thin Pt crystals, and J H Evans, Royal Holloway College, University of London, and H-E Schaefer, Institut für Theoretische und Angewandte Physik, Universität Stuttgart, for helpful discussions.

References

Evans J H and van Veen A 1989 *J. Nucl. Mater.* **168** 12
Goodhew P J and Tyler S K 1981 *Proc. R. Soc.* A **377** 151
Gråbaek L, Bohr J, Johnson E, Andersen H H, Johansen A and Sarholt-Kristensen L 1989 *Mater. Sci. Eng.* A **115** 97
Gråbaek L, Bohr J, Johnson E, Johansen A, Sarholt-Kristensen L and Andersen H H 1990 *Phys. Rev. Lett.* **64** 934
Horsewell A 1990 *Phil. Mag.* B **62** 647
Horsewell A, Johnson E and Bourdelle K K 1993 *Mater. Sci. Forum* **126–128** 647
Jensen K O, Eldrup M, Pedersen N J and Evans J H 1988 *J. Phys. F: Met. Phys.* **18** 1703
Johnson E, Johansen A, Thoft N B, Andersen H H and Sarholt-Kristensen L 1993 *Phil. Mag. Lett.* **68** 131
Kellog G L 1991 *Surf. Sci.* **246** 31
Kim K T and Welsch G 1990 *Mater. Lett.* **9** 295
Liu C L, Cohen J M, Adams J B and Voter A F 1991 *Surf. Sci.* **253** 334
MacKenzie I K 1983 *Positron Solid-State Physics* ed W Brandt and A Dupasquir (Amsterdam: North-Holland) p 196
Markworth A J 1973 *Metall. Trans.* **4** 2651
Mikhlin E Ya 1979 *Phys. Status Solidi* a **56** 763
Nash C P, Boyden F M, Whittig L D 1960 *J. Am. Chem. Soc.* **82** 6203
Nichols F A 1969 *J. Nucl. Mater.* **30** 143
Ravn H, Schulte W H, Rolfs C, Waanders F B and Kavanagh R W 1991 *Nucl. Instrum. Methods* B **58** 174
Rein G, Mehrer H and Maier K 1978 *Phys. Status Solidi* a **45** 253
Schmalzried H 1974 *Solid State Reactions* (Weinheim: Chemie)
Schmidt B 1992 *MSc Thesis* University of Copenhagen
Silcock J M 1955/56 *J. Inst. Met.* **84** 19
Templier C 1991 *Fundamental Aspects of Inert Gases in Solids (NATO ASI Series B 279)* ed S E Donelly and J H Evans (New York: Plenum) p 117

Uhrmacher M and Lieb K P 1992 *Nucl. Instrum. Methods* B **68** 175
Van Siclen C DeW and Wright R N 1993 *Phil. Mag.* A **67** 1
Yamaguchi H, Hashimoto I, Mitsuya H, Nakamura K, Yagi E and Iawki M 1989 *J. Nucl. Mater.* **161** 164
Zhang D L and Cantor B 1990 *Phil. Mag.* **62** 557
Ziegler J F, Biersack J P and Littmark U 1985 *The Stopping and Ranges of Ions in Solids* (New York: Pergamon)